Facile Photoelectrode Architecture of Porous Anodic Alumina for Dye-sensitized Solar Cells

[1]Chia-Tien Wu, [2]Chia-ChihHo and [3*]Fu-Hsiang Ko

Abatract

We introduce a new photo electrode architecture, fabricated through facile synthesis of self-organized hollow TiO_2nanocones under porous anodic alumina (PAA) featuring TiO_2 nanotubes (NTs) within. PAA was grown directly on a fluorine-doped tin oxide substrate, which provided good contact for PAA-based dye-sensitized solar cells (DSSCs). The TiO_2nanocones grew as anodization proceeded for the growth of the PAA and the underlying Ti, preventing the delamination of PAA from the substrate and the formation of an undesirable barrier layer. Ordered TiO_2 NT arrays were grown along the pore walls of the PAA by infiltrating with $Ti(OiPr)_4$. The hybrid structure was integrated into a DSSC device using a commercially available N719 dye. The cell incorporating hollow TiO_2 nanocones under PAA and TiO_2 NTs as the working electrode generated a photocurrent of 5.15 mA/cm^2, an open-circuit voltage of 0.64 V, and a power conversion efficiency of 1.71%—superior performance relative to those of corresponding TiO_2 NT/PAA and TiO_2 NT–alone devices.

Keywords: Nanotubes, Photoelectric Conversion, Nanoporous Materials, Nanostructured Materials in Electrochemistry.

1. Introduction

With the growing interest in green energy, solar cells have become a potential solution to mitigate the problems of global warming. Scientists and engineers are seeking next-generation photovoltaic systems exhibiting high efficiencies, low costs, and the possibility of high-throughput manufacture. Since the pioneering studies of Gratzel et al., dye-sensitized solar cells (DSSCs) have blossomed to have great potential for commercialization [1]. DSSCs provide some advantages over conventional solid state solar cells: insensitivity to oblique light incidence and temperature effects; very-low-cost, simple fabrication; transparency; and flexibility. DSSCs comprise four main building blocks: a photoanode of TiO_2 nanoparticles (NPs), a light-absorbing dye, an iodide electrolyte, and a Pt counter-electrode [2].

Department of Materials Science and Engineering, National Chiao-Tung University, Hsinchu 300, Taiwan
[*]E-mail: fhko@mail.nctu.edu.tw

Photo-excitation of the dye results in injection of electrons into the TiO_2 NPs while holes are released to the iodide/triiodide couples in the electrolyte. Carriers are transported in the conduction band of TiO_2 and diffuse to the charge collector of the transparent conductive oxide (TCO). The iodide is reduced to triiodide at the counter-electrode. The circuit is completed through electron migration through the external load [3].

In the past few years, increases in DSSC efficiencies have been attributed to improvements in the syntheses of ruthenium complex dyes and in the nanoscale architectures of the TiO_2 networks [4-5]. Several ruthenium dyes have been synthesized and provided excellent power conversion efficiencies (PCEs), some reaching greater than 11% [6-7]. Although the development of photoanodes has been relatively lagging, it remains one of the most promising avenues toward enhancing device performance. The ability to fabricate modern TiO_2 networks is expected to have a positive impact on solar cell performance by providing more-direct migration pathways with the improved charge transport efficiencies [8]. Porous networks of TiO_2 NPs typically serve as the photoanode of DSSCs on the surface of transparent conducting glass. Unfortunately, the broad distribution of interconnections resulting from a randomly packed NP network significantly retards the transport dynamics [9]. The structured disorder associated with the contacts of the TiO_2 NPs that enhance the scattering of free electrons, thereby reducing electron mobility [10].

Recently, TiO_2 nanotube (NT) arrays have been considered as alternative modern electrodes, replacing TiO_2 NPs, for highly efficient DSSCs [11-14]. TiO_2 NT arrays, which possess an ordered and strongly interconnected nanoscale photoanode architecture, provide superior electron lifetimes and more-direct migration pathways for electron percolation; they also result in markedly higher charge-collection efficiencies and light-harvesting efficiencies relative to those of traditional NP films. TiO_2 NT arrays are prepared through anodization of thick-film Ti foils or Ti films on transparent conducting glasses. Intuitively, NT-based DSSCs should have higher efficiencies than their NP-based counterparts. Practically, however, the overall conversion efficiencies that have been reported previously are similar for both types of film structures. The results are imputed to aggregation of the NTs, arising from the capillary forces, during the fabrication process. The individual NTs are transformed into clusters of bundled NTs during the

anodization process or electrolyte injection, and may be accompanied by cracking of the film. These similar phenomena have been observed for other one-dimensional nanostructures (e.g., Si nanowires and carbon NTs) [15]. The bundling of NTs, much like porous NP films, produces many unnecessary interconnections. These contacts substantially retard electron transport and the dye-loading capacity, thereby leading to poor efficiency [16].

Hupp and co-workers have developed one solution to this problem by separating the TiO_2 NTs using commercial porous anodic alumina (PAA) membranes [17-18]. The reactive gas precursor was coated into PAA conformably using an atomic layer deposition (ALD) system to form TiO_2 NTs along the pore wall. Kang et al. fabricated highly ordered TiO_2 NTs using the same PAA templating method [19]. A modified sol–gel route was used to infiltrate the commercial PAA with $Ti(OiPr)_4$, which was subsequently converted into TiO_2 NTs. The photovoltaic performance of such TiO_2/PAA cells was, however, barely acceptable. Theoretically, the separating of NTs without interconnection should improve electron transport, leading to higher photo efficiencies; in addition, the alumina layer should slow the recombination of photo generated electrons on the TiO_2 conduction band and holes in the electrolyte or the oxidized dye. An inherent problem to these devices is poor contact between commercial PAA and the TCO layer, resulting in a loss of current transportation. Besides, macro/micro-crack formation during the transfer of freestanding PAA films onto TCO substrates can also have a negative effect on photovoltaic performance. Growing PAA directly on TCO substrates might overcome the aforementioned problems. A uniform PAA, with sufficient adhesion to the TCO layer to withstand thermal and surface treatment, is imperative for DSSC fabrication [20-21]. Although promising in theory, practical implementation of this approach has two major challenges. The first is poor anodization on the Al/TCO bilayer, mainly due to poor adhesion between Al and TCO. When a noble metal or TCO serves as the underlying substrate, the evolution of gaseous O_2 produces stress that damages the PAA/TCO adhesion. As many previous reports have described the upper PAA eventually delaminates from the underlayer, which weaken the performance of the resulting cells [22-23]. The second major challenge is forming a thick alumina barrier at the interface between the PAA and the TCO layer [24-25]. The formation of PAA, either from Al foil or from Al and a substrate, accompanies a barrier layer at the bottom of the pore channels. The isolated barrier layer would prohibit the connection of the pore channels and the substrate. In the DSSC application, it would block current transport between the TiO_2 NTs and the TCO layer. It is because of the current density is inversely proportional to the exponent of barrier thickness for a given anodization voltage [26], the high current density produced by a highly conductive TCO would result in a thick alumina barrier. The alumina barrier would be difficult to remove selectively using dilute phosphoric acid while also widening the pores [27].

In this study, we overcome the challenges described above by using a 15-nm-Ti adhesion layer between the Al and the fluorine-doped tin oxide (FTO). During the Al anodization process, the underlying Ti was oxidized to form hollow TiO_2 nanocone arrays [28], which resulted in stable anodization and suppressed the formation of a thick barrier layer. After using a modified sol–gel process to deposit TiO_2 onto the pore wall of PAA, we developed a versatile technique for fabricating a new photo electrode architecture consisting of hollow TiO_2 nanocones under PAA with TiO_2 NTs inside. Photovoltaic performance in relation to the electrode geometry is also discussed.

2. Experimental

2.1 Chemicals, Materials and Al/Ti Bilayer Preparation

Phosphoric acid (86%), anhydrous EtOH (99.5%), hydrochloricacid (37%), 4-tert-butylpyridine (TBP, 96%), 3-methoxypropionitrile (MPN, 99%), and $Ti(OiPr)_4$ (97%) were purchased from Aldrich. Iodine (98%) and lithium iodide (99%) were purchased from J. T. Baker. A hot-molten film (SX-1170), FTO glass (10 Ω/sq, TCO10-10), and ruthenium 535-bis-TBA (N719) were purchased from Solaronix. Dihydrogen hexachloroplatinate (H_2PtCl_6) solution was purchased from Alfa Aesar. Ti (99.995%) and Al (99.995%) targets were purchased form Praxair. Ultrapure water was used in all experiments; it was purified by using a Milli-Q apparatus (Millipore) to a resistivity of 18.2 $M\Omega$ cm. All chemicals were used without further purification.

Ti (15 nm) and Al (1 μm) films were deposited sequentially onto cleaned FTO glass by using an ultrahigh vacuum DC sputtering system (ULVAC, SBH-3308). Prior to film deposition, the base pressure of the sputtering chamber, was adjusted to approximately 5×10^{-7} torr. Subsequently, the sample was annealed under Ar/H_2 ambient at 400 °C for 2 h to reduce the defects and improved the adhesion. The Al/Ti/FTO sample then was polished electrochemically (20 V, 1 °C) in a vigorously stirred mixture of $HClO_4$ and EtOH (1:4) to reduce the surface roughness during high-field anodization.

2.2 Anodization Process and Synthesis of TiO$_2$ NTs

Anodization was performed at 1 ℃ in a glass beaker, cooled by a powerful cooling system and with vigorous magnetic stirring. A DC power supply connected to a computer system was used to vary the potential and current during anodization. Cu foil was used as a support for the working electrode. The substrate was positioned on top of the support; Cu tape was used to connect the Cu support to the Al film on the sample. Two acrylic caps were used to fasten the sample and the Cu support within an O-ring. A graphite flake was used as the counter electrode. The anodizing process was performed in an electrolyte of 1.0 M H$_3$PO$_4$ at a constant voltage of 86 V. Anodization was terminated once the current decreased to the background level and the color of the sample changed from opaque to transparent. When the anodization was complete, hollow TiO$_2$ nanocones were also formed at the bottom of the PAA pores.

Titanium isopropoxide (5 mL) was added to absolute EtOH (25 mL) with vigorous magnetic stirring while maintaining the temperature at 1 ℃. Separately, water (0.5 mL) and 0.1 mol/L HCl (0.5 mL) were added to EtOH (25 mL). Thereupon, the Ti(OiPr)$_4$/EtOH sol was slowly added to the EtOH/HCl/H2O mixture at room temperature. After the resulting gel solution turned a milky color (60 s of homogenization), the PAA/FTO substrates (subjected to pre-treatment with EtOH) were immediately immersed into the gel solution for 1 min to form TiO$_2$ NTs. The residual gel solution on the back of the sample was washed away with EtOH. After drying in air at room temperature, the sample was placed in a furnace, heated at a rate of 2 ℃/min up to 450 ℃, and held at that temperature for 5 h to crystallize it into anatase TiO$_2$.

2.3 Cell Assembly and Characterization

The sample was sensitized in absolute EtOH solution containing 6.7 x 10^{-4} M N719 dye for 12 h. The dyed electrodes were rinsed with absolute EtOH and dried under a N$_2$ stream. A Pt counter electrode was prepared by spin-coating H$_2$PtCl$_6$ solution onto the FTO glass and then sintering it at 450 ℃ for 30 min. The dye-covered TiO$_2$ electrode and Pt counter electrode were assembled into a sandwich-type cell. The electrode spacing between them was sealed using a 25-μm-thick hot-molten film as a spacer. The electrolyte (0.5 M LiI, 0.05 M I$_2$, and 0.5 M TBP in MPN) was introduced into the cell through a hole (diameter: 1 mm) drilled in the counter electrode. A second spacer was sealed over the hole by using a soldering iron. Figure 1 provides a representation of such an assembled DSSC device.

The morphology was observed using a field-emission scanning electron microscope (JEOL, JSE-6700F). Grazing-incidence X-ray diffraction (GIXRD, PANalytical X'Pert Pro system) was used to examine the composition. A one-sun AM-1.5 solar simulator (Sciencetech, SF150) served as the standard light source for the photovoltaic devices. The current–voltage characteristics were examined using Keithley 2400 source-meter instruments with a probe station system. UV−Vis spectroscopy (Hitachi, U3100) was used to measure the absorption of the organic materials.
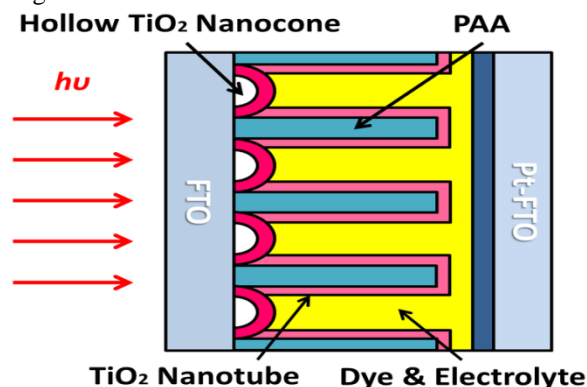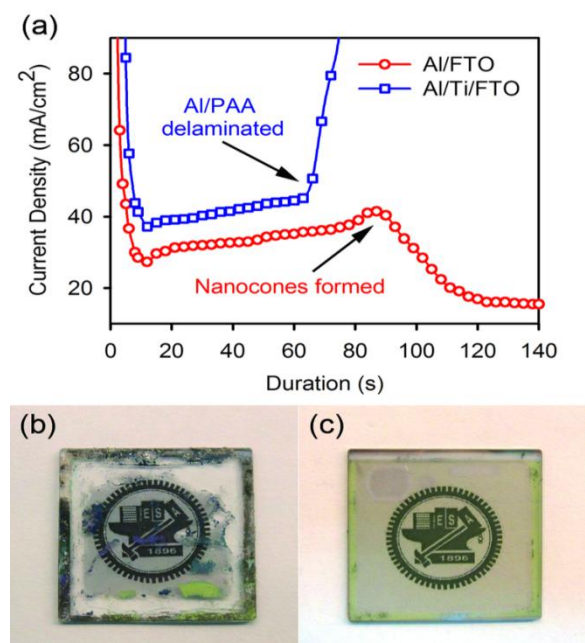

Figure 1: Representation of our assembled DSSC featuring TiO$_2$ NTs and nanocones within PAA.

3. Results and discussion

3.1 Anodizing behavior on FTO glass substrate

In many nanostructured electro-optical device designs, the desired configuration features of PAA are grown directly on a TCO substrate. As mentioned above, anodization of an Al/TCO substrate in the absence of a retardant layer suffers from a delamination problem. To solve the problem, we deposited a 15-nm-thick Ti layer between Al and the FTO. Figure 2(a) presents chronoamperic curves recorded during the anodization of Al on bare FTO glass and on FTO glass coated with a Ti layer. During the first stage, the initial decreases in current were due to barrier layer formation, followed by an escalation in current. When the anodizing time reached ca. 60 s, a sudden surge occurred in the current of the Al/FTO sample that was accompanied by sparks, gas evolution, and delamination, resulting from anodic breakdown of the FTO. The current then remained at a very high level as a result of direct contact between the FTO and the electrolyte. In contrast, when the 15-nm-thick Ti layer was present, the anodization current was noticeably stabilized, allowing anodization to proceed smoothly down to the substrate. Because Ti has a higher ionic conductivity than Al, anodic titanium oxide formed

preferentially, resulting in an increasing surge of current density. Once a visible change in color of the sample from opaque to transparent had occurred, the current density dropped to the base level. Figs. 2(b)-(c) display photographs of the final samples. Several obvious defects appear on the Al/FTO sample. The regions of limpid appearance were bare FTO; the dissolution reaction escalated as more areas of the FTO glass were exposed. That cause eventual delamination of PAA from the FTO glass. The regions with residual Al featured a metallic color. The complete formation of PAA resulted in the uniform transparency of the Al/Ti/FTO sample, which featured appropriate adhesion of PAA to the FTO substrate for the fabrication of DSSC devices.


Figure2: Representation of our assembled DSSC featuring TiO$_2$ NTs and nanocones within PAA.

3.2 Synthesis and characterization of hollow TiO2 nanocones

Figure 3(a) presents a top-view SEM image of self-organized hollow TiO$_2$nanocones after removing the upper alumina layer. The average geometric features of the quasi-closely-packed nanocone arrays were a period of 200 nm, a base diameter of 180 nm, and a density of 2×10^9 cm^{-2}. We used an FIB milling technique to expose the inner portion of the nanocones. The left-hand region in the image reveals 20-nm-thick shells with a hollow interior. After annealing at 450 °C, we used GIXRD analysis to confirm that these nanostructures were composed of anatase TiO$_2$ (Figure 3(f)). As the anodization process was completed, TiO$_2$ hollow nanocones were also formed in the bottom of PAA pores. The upper PAA was selectively removed by using a solution of 5 wt% H$_3$PO$_4$ and 45g/L chromic acid at 50 °C for 15

min. Subsequently, the sample was conducted in a furnace with a heating rate of 2 °C /min and kept at 450 °C for 5 h to crystalize into anatase TiO$_2$. A blank FTO substrate was used as a reference. Pronounced peaks of anatase TiO$_2$ were observed. This indicates the desirable crystal structure of nanocones. We expected that such transparent hollow TiO$_2$ nanostructures organized on TCO glass as an electrode would increase the contact area with the TCO substrate and, hence, provide efficient electron transport [29]. Films constructed of oriented one-dimensional nanostructures aligned perpendicular to the collecting TCO substrate could also improve the charge-collection efficiency by promoting faster transport and slower recombination [30]. Furthermore, in many PAA-based solar cells, NTs attached directly to TCO glass result in electrical shorting when the redox electrolyte came into direct contact with the TCO layer. In contrast, we expected our nanocone layer to serve as an insulating layer to avoid direct contact between the electrolyte and the TCO glass.
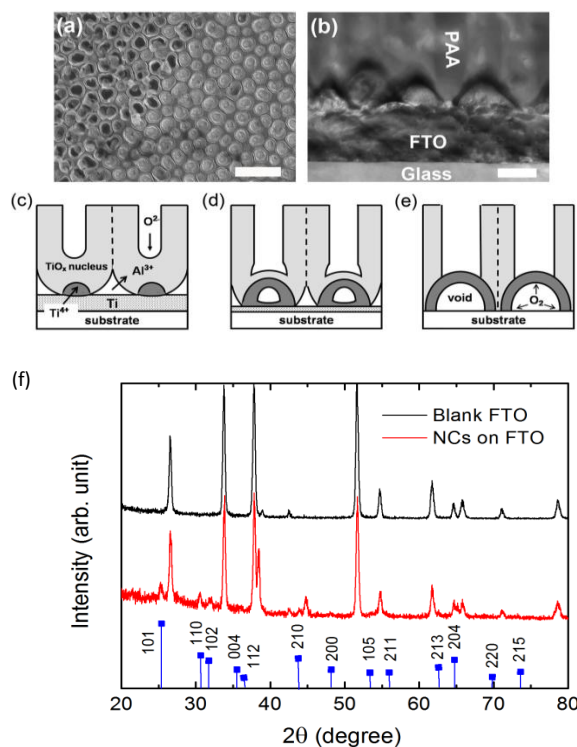
Figure 3: (a) Top-view SEM image (scale bar: 500 nm) of hollow TiO$_2$ nanocone arrays after alumina had been removed selectively. In the left part of the image focused ion beam (FIB) milling had been used to reveal the hollow inner sections of the nanocones. (b) Cross-sectional TEM image of hollow TiO$_2$ nanocones (scale bar: 100 nm). (c)-(e) Schematic representation of the mechanism of formation of the hollow nanocones. (c) TiO$_2$ nucleus formed as the anodization approached the Ti–Al interface. (d)

TiO$_2$ hillocks grew, leaving voids caused by O$_2$ pressure. (e) Cone-like hollow nanostructures formed with obstructing pore-walls. (f) Grazing incident X-ray diffraction (GIXRD) analysis for TiO$_2$nanocones on FTO.

We used TEM to investigate the morphologies of the contact interfaces between the nanocones, the substrate, and alumina wall (figure 3(b)). An isolated hollow nanostructure was embedded at the bottom of each alumina pore, i.e., at the interface between the porous alumina and the substrate. Notably, no barrier layer was evident—a very advantageous situation for the subsequent deposition of TiO$_2$ NTs. The PAA was aligned perpendicular to the substrate, with self-organized hollow TiO$_2$nanocones at a height of 150 nm. We suspected that having the ability to control the nanoscale architecture of the TiO$_2$ network would positively impact solar cell performance by providing more-direct migration pathways with improved charge transport efficiencies, as well as simplified device architectures [31]. Template-directed synthesis is an ideal tool for fabricating oxide NTs because their physical dimensions can be controlled precisely and monodisperse samples can be harvested in large quantity. Our PAA template consisted of well-aligned, uniform, cylindrical pores. With good adhesion to the FTO glass, making them highly suitable for subsequent TiO$_2$ sol–gel synthesis.

Combining the chronoamperical data with the microscopy images, Figs. 3(c)–(e) presents a proposed mechanism of formation for the TiO$_2$ nanocones. If a metal whose oxide form has a higher ionic conductivity than alumina was used as an underlayer preceding an Al anodization process, the underlying metal would be also oxidized and thereby form metal–oxide nanostructures with a similar pattern as the upper PAA [32-34]. Metal-oxide nanostructures formed between the pores of PAA and the substrate are referred to as the oxidation of metal layer. The O^{2-} ions migrating inward through the alumina barrier layer were injected into the metal layer, forming the metal-oxide nucleus (figure. 3(c)). When the anodization front approached the Ti–Al interface, anodization of the underlying Ti began. The O^{2-} ions migrating inward through the alumina barrier layer were injected into the Ti layer to form a tantalum oxide nucleus. The growth (volume expansion) of the tantalum oxide nanostructure resulted from the continuous combination of O^{2-} and Ti^{4+} ions. We found, however, that the excess of O^{2-} ions was relative to the limited amount of 15-nm-thick Ti, and combined to release O$_2$ gas at the anode. The gaseous O$_2$, acted as a porogen, exerted great pressure to expand the tantalum oxide hillocks, and let a void between them and the underlying substrate (figure 3(d)) [23]. The stress produced by O$_2$ gas resulted in the formation of a void under each pore of the anodic PAA [28]. During the formation of

titaniananocones, the alumina wall and barrier were continuously thinned by H$_3$PO$_4$ electrolyte itself. As the voids expanded, as a result of the effects of gaseous O$_2$, the barrier layers eventually dissolved entirely and the hollow hillocks grew upward. With the obstructing pore wall, cone-like hollow nanostructures were ultimately obtained (Figure 3(e)).

3.3 Synthesis and characterization of TiO$_2$ NTs

A typical sol solution of Ti(OiPr)$_4$ includes both EtOH and water with a variety of other additives. The water acts to hydrolyze Ti(OiPr)$_4$, leading to the formation of TiO$_2$ particulates in solution through a series of condensation reactions, which, when brought to completion. That resulted in the formation of the gel. Figs. 4(a)-(b) display top-view SEM images of PAA before and after performing the Ti(OiPr)$_4$ sol–gel process. The average geometric features of blank PAA were a period of 200 nm, a height of 1.2 μm, and a density of 2 x 10^9 cm^{-2}. Comparing Figs. 4a and 4b reveals that hollow TiO$_2$ gel structures were formed within the pore walls of the PAA; the pore diameters in these two images (ca. 160 and 120 nm respectively) suggest that the wall thickness of the deposited TiO$_2$ NTs was ca. 20 nm. The TiO$_2$ NT layer adhered to the pore wall tightly without forming cracks. Thus, the TiO$_2$ sol flowed into the pores along the pore wall of the PAA through an infiltration process, due to surface tension and capillary effects. Notably, the affinitive treatment in EtOH for PAA was a necessary step for achieving hollow TiO$_2$ gel structures; otherwise, shrinking or cracking would occur to separate the NTs from the pore walls during the subsequent heating process.
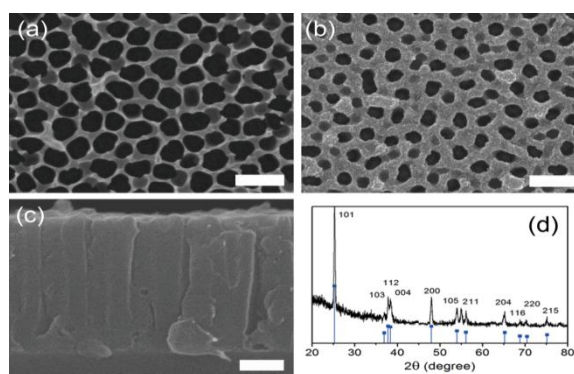
Figure4: **(a)-(c) Morphology of the TiO$_2$ NTs grown onto the pore walls of PAA. (a)-(b) Top-view SEM images (scale bar: 500 nm) of PAA (a) before and (b) after deposition of the TiO$_2$ NTs. (c) Cross-sectional SEM image (scale bar: 200 nm) of the sample in (b). (d) GIXRD analysis of a TiO$_2$ NT, revealing the desirable crystalline anatase phase.**

Figure 4(c) reveals that TiO_2 NTs were hollow and grew along the PAA template to self-organize into hollow TiO2 nanocones. With the aid of PAA, the TiO_2 NTs were formed without the bundling or microcracking that has been reported previously [15-16]. This architecture allows electrons to transfer in a more direct route through the well-aligned pathways of the TiO_2 NTs, presumably improving the performance of the DSSC. The arrangement of the highly ordered TiO_2 NT array perpendicular to the surface permits facile charge transfer along the length of the NT from the solution to the conductive substrate, thereby reducing the losses incurred by charge hopping across NP grain boundaries. An easier access to the NT array surface, as well as better control of the interface, makes this morphology desirable for DSSCs. An enhanced electron transport also allows the improved light harvesting because thicker films can be used to increase the optical density, which improved the absorption of low-energy photons in the red and infrared spectral regions without losing the additionally harvested charge carriers to recombination.

Anatase-phase TiO_2 is a good candidate for use as a photoelectrode. We converted the as-deposited amorphous TiO_2 NTs to the anatase phase by annealing the sample at 450 °C in O_2 for 5 h. Notably, GIXRD analysis (Figure 4(d)) provided no evidence of the rutile phase. The enhanced (101) peak at a value of 2θ of 25.3° reveals that the NTs were well crystallized. An average crystallite size of 28 nm was estimated from the Scherrer equation.
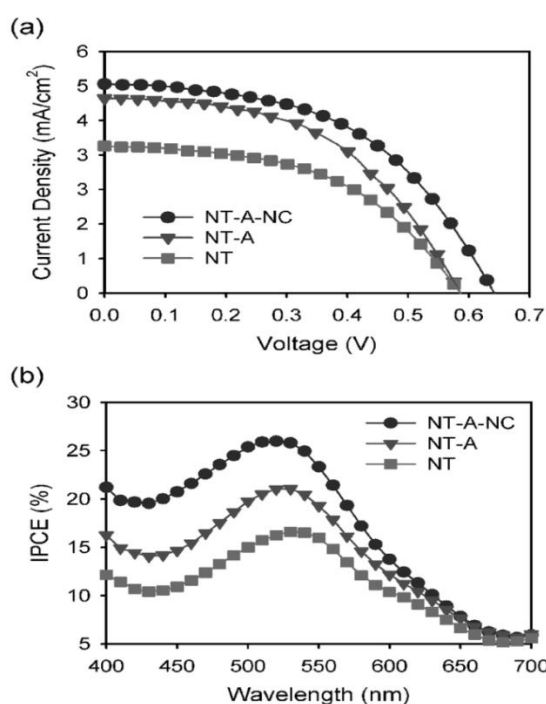
3.4 Photovoltaic performance

We investigated the effect of the electrode morphology on the performance of DSSCs by comparing cells featuring different working electrode structures: hollow TiO_2 nanocones under porous alumina and TiO_2 NTs (NT-A-NC); a TiO_2 film under porous alumina and TiO_2 NTs (NT-A); and anodic TiO_2 NTs without alumina (NT). Samples NT-A-NC and NT-A in Figure 5 allowed us to discern the effect of the hollow TiO_2 nanocones; samples NT-A and NT allowed us to verify the role of the anodic aluminum oxide in the DSSC. A TiO_2 film was substituted for TiO_2 nanocones under porous alumina in sample NT-A-NC. The TiO_2 film electrode was prepared by the sol-gel spin-coating method. Titanium isopropoxide (5 mL) was added to absolute EtOH (25 mL) maintaining the temperature at 1 °C. Separately, water (0.5 mL) and 0.1 mol/L HCl (0.5 mL) were added to EtOH (25 mL). Thereupon, the Ti(OiPr)$_4$/EtOH sol was slowly added to the EtOH/HCl/H_2O mixture. The result of gel solution was spun onto FTO substrates. After drying in air at room temperature, the sample was placed in a furnace, heated at a rate of 2 °C/min up to 450 °C, and held at that temperature for 5 h. An only Al film was deposited onto TiO_2/FTO substrate after. The

arithmetic average roughness (R_a) and root mean square roughness (R_{RMS}) were 2.45 and 5.13 nm, respectively. The thickness of TiO_2 film is 100 nm from cross-sectional SEM observation. Anodic TiO_2 NTs were substituted for sol-gel TiO_2 NTs within PAA in samples NT-A-NC and NT-A. The anodic TiO_2 NTs were prepared by direct anodization of Ti film (800 nm) deposited onto FTO substrate. The anodizing process was performed in an electrolyte of 0.25 wt% NH4F and ethylene glycol (99.8% anhydrous) solution at a constant voltage of 60 V. The sample was then placed in a furnace, heated at a rate of 2 °C/min up to 450 °C, and held at that temperature for 5 h.The average inner diameter of the nanotube was 110 nm and outer diameter 160 nm. The depth of anodic TiO_2 NTs was estimated at about 700 nm from cross-sectional SEM observation. As we can see, cracks and interconnections appear in TiO_2 NTs. The standard back contact used was FTO glass; the standard counter electrode was Pt-coated FTO glass. A panchromatic sensitizer, N719 dye, was used as the standard dye; the standard high-boiling-point iodide-based electrolyte (in MPN) was employed. Photovoltaic measurements were performed using an AM 1.5 solar simulator equipped with a 150-W Xe lamp; the power of the simulated light was calibrated to 100 mW/cm^2. The photocurrent (I) and photovoltage (V) of the cell were measured over an active area of 0.25 cm^2.
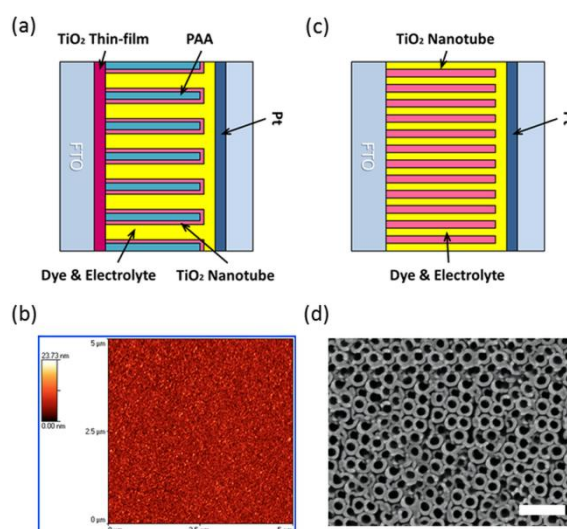
Figure5: **Schematic and microscopic images of samples NT-A-NC and NT-A.(a) Schematic representation of sample NT-A.A TiO_2 film was substituted for TiO_2nanocones under porous alumina in sample NT-A-NC.(b) The AFM image of TiO_2 film onto FTO substrate.(c) Schematic representation of sample NT.(d) Top-view SEM image (scale bar: 500 nm) of anodic TiO_2 NTs of sample NT.**

Figure 6(a) displays representative current–voltage (I–V) data for the DSSCs; Table 1 lists the photovoltaic performance parameters. We should notice that all TiO_2 nanotubes in these three samples are indentical in length, which enables the comparsion and discussion with the same criterion. For sample NT-A-NC, the device exhibited an open-circuit voltage (Voc) of 0.64 V, a short-circuit current density (Jsc) of 5.15 mA/cm^2, and a fill factor (FF) of 0.59, which give an overall power conversion efficiency (η) of 1.71%. For sample NT-A, of which the TiO_2 film replaced the TiO_2 nanocones as the electrode, these values were all lower. Thus, the hollow TiO_2 nanocones played a predominant role in enhancing the photoconversion efficiency. We suspect that the nanocone structures increased the contact area with the TCO substrate, thereby enhancing electron transport, as reflected by the higher value of Jsc [30]. A recent study has revealed that hollow TiO_2 can greatly enhance the photocatalytic activity or photoelectric conversion efficiency as a result of the multiple reflection of light [29, 31]; for the same reason, we believe that the larger value of Jsc for sample NT-A-NC arose from enhanced light harvesting, due to multiple light reflection and scattering between the shells of the self-organized hollow TiO_2 nanocones. In addition, the electron transport path through a hollow cone-like electrode is different from that in a thin film. Because the electrons transferred from the NTs to the FTO layer along the thin TiO_2 shell, the structure provided shorter and more-direct transport paths for electrons, compared with those for the TiO_2 film in sample NT-A, resulting in a greater value of Voc [30].

morphologies as electrodes: hollow TiO_2 nanocones under porous alumina and TiO_2 NTs (NT-A-NC); a TiO_2 film under porous alumina and TiO_2 NTs (NT-A); and anodic TiO_2 NTs without alumina (NT). (a) Current–voltage characteristics of the three DSSC devices. (b) The incident photon–to–current conversion efficiency (IPCE) spectra of the three DSSC devices.

To verify the role of porous alumina in DSSC, we compared the performances of sample NT-A (with PAA) and sample NT (without PAA). Because the outer TiO_2 NTs were shielded by the inner PAA wall from the redox electrolyte, the rate of recombination in the NT-A structure was reduced [17-18]. Sample NT-A resulted in a 20% improvement in efficiency, from 1.22 to 1.45%. This reveal that the porous alumina acted as an insulating barrier between the TiO_2 NTs and the dye/electrolyte interface. Furthermore, clumps and cracklike features in TiO_2 NTs have, in fact, been observed (for details, see supplementary data). Clusters of bundled TiO_2 NTs could be produced during the anodization of Ti, thereby slowing down the electron transport dynamics in the electrodes. In contrast, with the aid of PAA, the TiO_2 NTs were presented without any bundling or microcracking, thereby providing electrons with a direct pathway toward the FTO glass.

Table 1: DSSC performance metrics

Sample	J_{sc} (mA/cm^2)	V_{oc} (V)	FF (%)	η (%)
NT-A-NC	5.15	0.64	59	1.71
NT-A	4.78	0.59	46	1.45
NT	3.62	0.60	47	1.22

Figure 6(b) presents action spectra for the incident photon–to–current conversion efficiency (IPCE) of the DSSC devices featuring the three different electrode structures. IPCE is defined as the number of generated electrons divided by the number of incident photons. Essentially, the IPCE intensities were systematically enlarged upon the same dye coinciding with the performances listed in Table 1. The IPCE spectra exhibited a peak of ca. 26% at 530 nm and an inflection point at 430 nm in relatively close agreement with the expected maximum based on the accompanying absorption spectrum for the N719 dye, which has local maxima at 377 and 526

Figure 6: Photovoltage performances of cells constructed with various TiO_2

nm in Figure 7, both corresponding to a metal-to-ligand charge transfer transitions. The absorption band in the UV region is due to the intraligand charge transfer transitions (ILCT). Also, the electronic absorption spectrum of N719 shows the characteristic metal-to-ligand charge-transfer transition (MLCT) absorption bands in the visible region at 527 nm. The molar extinction coefficients of MLCT absorption band for N719 dye is 1.36×10^4 M^{-1} cm^{-1}, which is as well as that of ILCT absorption band (1.36×10^4 M^{-1} cm^{-1}). When PAA was applied to the thin-film electrode devices, the IPCE peak height at 530 nm increased from 16 to 21%; the presence of the nanocone electrode promoted the value from 21 to 26%. It is interestingly noted that the IPCE increment of sample NT-A-NC (compared with sample NT) in near-UV region is larger than that of sample NT-A. The results indicated that light harvesting from reflection and scattering was reinforced by the nanocone array since the two absorption peaks of N719 dye in Figure S3 are identical in value.

The photovoltaic performances of these DSSC devices are similar to those of DSSCs featuring the same N719 dye and a titania NT electrode fabricated through deposition in a commercial PAA template. Note that the average length of the titania NTs in commercial PAA was greater than 20 μm; i.e., they were much longer than the ones we prepared in this study. In general, higher efficiencies result when using NTs of greater lengths. For example, Varghese et al. found that the power conversion efficiency improved from 2.6 to 6.9% when the average length of the titania NTs increased from 1.2 to 20 μm. Therefore, we believe that the improvement in the power conversion efficiency of our cells resulted from the formation of uniform Al films (tens of micrometers thick) on the FTO glass. Also, the $TiCl_4$ treatment to NTs is able to enhance the photogenerated current and the power conversion efficiency [11].
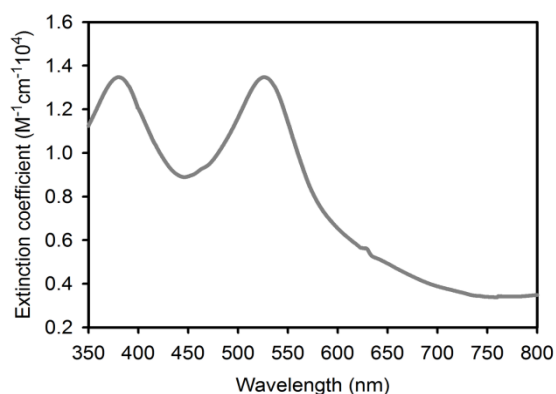
Figure7: Absorption spectra of N719 sensitizer in absolute ethanol solution.

4. Conclusions

We have fabricated hollow TiO2 nanocones under PAA featuring TiO_2 NTs within directly on FTO glass and used them as new working electrodes in DSSCs. By depositing a thin layer (15-nm-thick) of Ti on a FTO substrate prior to anodization, we obtained self-organized hollow TiO_2 nanocones with the improved contact between the FTO substrate and the overlaying Al. Thereby it can solve the problems of delamination of an undesirable barrier. This more-stable, barrier-free PAA/FTO structure was highly suitable for use in subsequent sol–gel processing of $Ti(OiPr)_4$. The novel structure combines two types of TiO_2 materials—0-D nanocones and 1-D NTs—may benefit from a large contact area, direct electron transport path, and slow recombination of electrons. The relatively short NT array (1.2 μm) results in a considerably lower photoabsorption than, for example, the current DSSC "gold standard" featuring a tens-of-micrometers-thick layer of TiO_2 NTs. We suspect that increasing the length of the NT array on the electrode might allow us to further improve the efficiencies of such DSSCs. The facile synthesis of this novel architecture may allow the design of new nanostructures for use as new building blocks in future electro-optical devices.

Acknowledgments

References

[1] B. Oregan, M.Gratzel,*Nature*, 353 (1991) 737-40.
[2] M. Gratzel,*Nature*, 414 (2001) 338-44.
[3] M. Gratzel,*Inorg. Chem.*, 44 (2005) 6841-51.
[4] L. M. Peter, *J. Phys. Chem. C*, 111 (2007) 6601-12.
[5] M. Gratzel,*Acc. Chem. Res.*, 42 (2009) 1788-98.
[6] C. Y. Chen, M. K. Wang, J. Y. Li, N.Pootrakulchote, L.Alibabaei, C. H.Ngocle, J. D.Decoppet, J. H. Tsai, C.Gratzel, C. G. Wu, S. M.Zakeeruddin, M.Gratzel,*ACS Nano*, 3 (2009) 3103-9.
[7] T. Bessho, S. M.Zakeeruddin, C. Y.Yeh, E. W. G.Diau, M.Gratzel,*Angew. Chem.Int. Ed.*, 49 (2010) 6646-9.
[8] L. M. Peter, N. W. Duffy, R. L. Wang, K. G. U.Wijayantha,*J. Electroanal. Chem.*, 524 (2002) 127-36.

[9] N. Kopidakis, K. D.Benkstein, J. van de Lagemaat, A. Frank,*J. Phys. Chem. B*, 107(2003) 11307-15.

[10]M. Law, L. E. Greene, J. C. Johnson, R.Saykally, P. D. Yang,*Nat. Mater.*, 4 (2005) 455-9.

[11]G. K. Mor, K. Shankar, M.Paulose, O. K. Varghese, C. A. Grimes,*Nano Lett.*, 6 (2006) 215-8.

[12]K. Zhu, N. R. Neale, A.Miedaner, A.J. Frank,*Nano Lett.*, 7 (2007) 69-74.

[13]O. K. Varghese, M.Paulose, C. A. Grimes,*Nat. Nanotechnol.*, 4 (2009) 592-7.

[14]L. L. Li, C. Y. Tsai, H. P. Wu, C. C. Chen, E. W. G.Diau,*J. Mater. Chem.*, 20 (2010) 2753-8.

[15]D. Kim, A.Ghicov, P.Schmuki,*Electrochem. Commun.*, 10 (2008) 1835-8.

[16]K. Zhu, T. B.Vinzant, N. R. Neale, A. J. Frank,*Nano Lett.*, 7 (2007) 3739-46.

[17]A. B. F. Martinson, J. W. Elam, J. T.Hupp, M. J.Pellin,*Nano Lett.*, 7 (2007) 2183-7.

[18]A. B. F. Martinson, J. W. Elam, J. Liu, M. J.Pellin, T. J. Marks, J. T.Hupp,*Nano Lett.*, 8 (2008) 2862-6.

[19]T. S. Kang, A. P. Smith, B. E. Taylor, M. F.Durstock,*Nano Lett.*, 9 (2009) 601-6.

[20]N. N. Bwana,*Curr. Appl. Phys.*, 9 (2009) 104-7.

[21]L. K. Tan, M. K. Kumar, W. W. An, H.Gao,*ACS Appl. Mater. Interfaces*, 2 (2010) 498-503.

[22]S. Z. Chu, K. Wada, S. Inoue, S.Todoroki,*J. Electrochem. Soc.*, 149 (2002) B321-7.

[23]S. Z. Chu, K. Wada, S. Inoue, S.Todoroki,*Chem. Mater.*, 14 (2002) 266-72.

[24]T. R. B. Foong, A.Sellinger, X. Hu,*ACS Nano*, 2 (2008) 2250-6.

[25]P. A. Liu, V. P. Singh, S.Rajaputra,*Nanotechnology*, 21 (2010) 115303.

[26]N. Cabrera, N. F. Mott,*Rep. Prog. Phys.*, 12 (1949) 163-84.

[27]M. M. Crouse, A. E. Miller, D. T. Crouse, A. A.Ikram,*J. Electrochem. Soc.*, 152 (2005) D167-72.

[28]C. T. Wu, C. H. Lin, C. Cheng, C. S. Wu, H. C. Ting, F. C. Chang, F. H.Ko,*Chem. Mater.*, 22 (2010) 6583-9.

[29]H. J. Koo, Y. J. Kim, Y. H. Lee, W. I. Lee, K. Kim, N. G. Park,*Adv. Mater.*, 20 (2008) 195-9.

[30]S. C. Yang, D. J. Yang, J. Kim, J. M. Hong, H. G. Kim, I. D. Kim, H. Lee,*Adv. Mater.*, 20 (2008) 1059-64.

[31]Y. Kondo, H. Yoshikawa, K.Awaga, M. Murayama, T. Mori, K.Sunada, S.Bandow, S.Iijima,*Langmuir*, 24 (2008) 547-50.

[32]C. T. Wu, F. H.Ko, H. Y. Hwang,*Microelectron. Eng.*, 83 (2006) 1567-70.

[33]C. T.Wu, F. H.Ko, C. H. Lin,*Appl. Phys. Lett.*, 90 (2007) 171911.

[34]J. Oh, C. V. Thompson,*Adv. Mater.*, 20 (2008) 1368-72.